Foamed Gel Barriers in Porous Media: Breakdown and Permeability Evolution

Matthew J. Miller and H. Scott Fogler
Dept. of Chemical Engineering, The University of Michigan, Ann Arbor, MI 48109

Foamed gel has begun to play an important role in permeability modification applications because of the reduced chemical requirements. Foamed gels create impermeable barriers in porous media; however, once a critical pressure differential is exceeded, the permeability increases with increasing pressure. A two-dimensional network model was developed to estimate foamed gel barrier performance in terms of the maximum pressure a barrier can withstand and the evolution of the foamed gel barrier's permeability. The formation of conductive pathways and the accompanying permeability increase were estimated from a model of the pressure-induced deformation and rupture of individual lenses. The evolution of conductive pathways changed from invasion percolation (high elastic modulus, rigid gel) to a lens rupture chain reaction initiated by the rupture of a single lens (low elastic modulus gel) as the elastic modulus of the gel was decreased. The apparent fractal dimension of the first conductive channel ranged from 1.89 to 1.06 for high and low elastic modulus gels, respectively. This dependency of breakthrough and breakdown is unique and produces a large range of breakdown behavior for any degree of microscopic heterogeneity.

Introduction

Foam has long been recognized as a means of creating structures from a minimum of raw material. Foamed plastics are widely used because they are lightweight and inexpensive in comparison to the same object manufactured from nonfoamed plastic (Oertel, 1985). Foamed cements are used for a variety of applications including construction and cementing oil well casings because they are significantly less dense than solid cement, yet remain sufficiently strong (Tonyan and Gibson, 1992a, b; Benge et al., 1982). More recently, gel used to plug the conductive pore space of porous media has been foamed to reduce the material requirements. Foamed gel is generated in the pore space by the simultaneous injection of gas and a gelling solution (water soluble polymers with multivalent ion cross-linkers) and after gelation exists as a gelled phase with an interdispersed gas phase, similar to an aqueous foam whose external phase has undergone a polymerization reaction. Foamed gels have been used in the plugging of high conductivity streaks to modify the injection profile of oil wells, the stabilization of earthen formations, and the formation of impermeable barriers to divert groundwater flow away from contaminant plumes (Douben, 1970; Sydansk, 1992; Clampitt, 1981; Hazlett and Shu, 1989; Ali, 1992; Chmilowski and Kondratoff, 1992; de Rozieres and Ferriere, 1991). In a previous article we demonstrated that foamed gel barriers in porous media fail when exposed to excessive stress (Miller and Fogler, 1992). For effective use as a matrix permeability modifier, one must be able to estimate a foamed gel barrier's failure stress (barrier rupture pressure) and its permeability after failure. This article presents a model of the breakdown of foamed gel barriers and provides estimates of the barrier rupture pressure and barrier permeability.

Foamed Gel Breakdown

After injection and gelation in porous media, the foamed gel coats the pore body walls and occupies the pore throat constrictions in the form of gelled lenses, thus encapsulating gas as depicted in Figure 1. It has been shown that gas cells trapped in porous media span at least one pore body (Ettinger and Radke, 1992). Although foamed gel efficiently renders porous media virtually impermeable, the permeability of the treated zone increases irreversibly once the pressure drop across the foamed gel barrier exceeds a critical barrier rupture pressure, similar to systems exhibiting threshold behavior such as dielectric breakdown, and flow of Bingham plas-

Correspondence concerning this article should be addressed to H. S. Fogler.

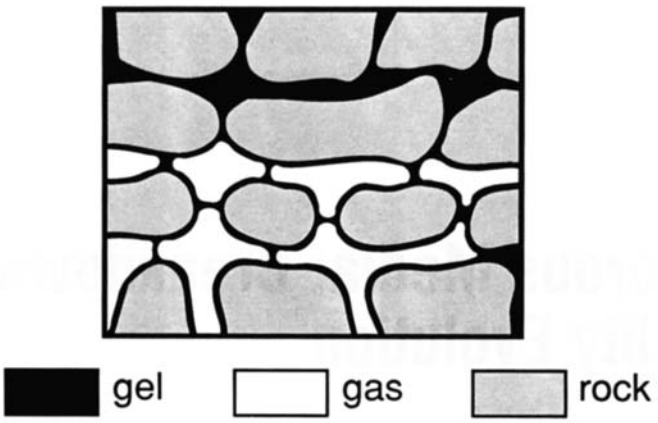

Figure 1. Foamed gel filled pore space.

tics through porous media (Roux et al., 1987; Rossen and Mamun, 1993; Sahimi, 1993). At the pore level, the gelled lenses deform when a pressure drop is imposed across the foamed gel bank (illustrated in Figure 2a). Microvisual experiments showed that the rupture of successive gelled lenses led to the formation of a conductive channel at the barrier rupture pressure as shown in Figure 2b. Although the permeability increases once channels percolate the foamed gel barrier, the permeability loss remains significant as pores 100% saturated with gel, intact lenses, and gel debris continue to restrict fluid flow. A pore body becomes 100% saturated with the gelling solution if the local capillary pressure is less than the capillary entry pressure of gas into the pore throats surrounding that pore body. Gel debris is gel that remains adhered to the pore throat walls after lens rupture and restricts fluid flow. As the injection pressure rises above the barrier rupture pressure, additional lenses rupture, increasing the number of conductive channels and the medium's effective permeability, as shown in Figure 3. The physical properties of individual gelled lenses (the gel strength, foam quality, and pore throat size) have a significant effect on the barrier rupture pressure, and the evolution of the post-treatment permeability (Miller and Fogler, 1992).

The foamed gel breakdown (FGB) curve provides important information about foamed gel barrier performance such as the maximum pressure the barrier can withstand without failing and the evolution of barrier permeability due to pressure-induced breakdown of the foamed gel structure. A model that estimates the complete foamed gel breakdown curve

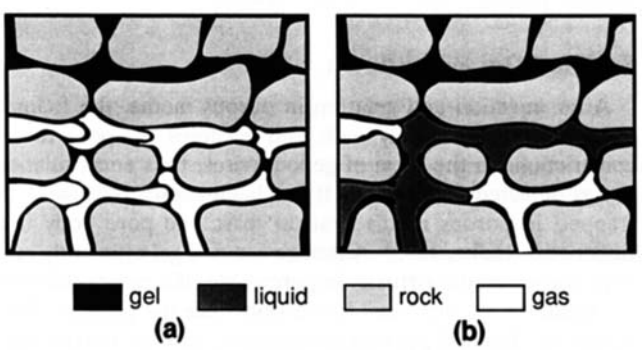

Figure 2. Foamed gel: (a) under applied force; (b) with a conductive channel.

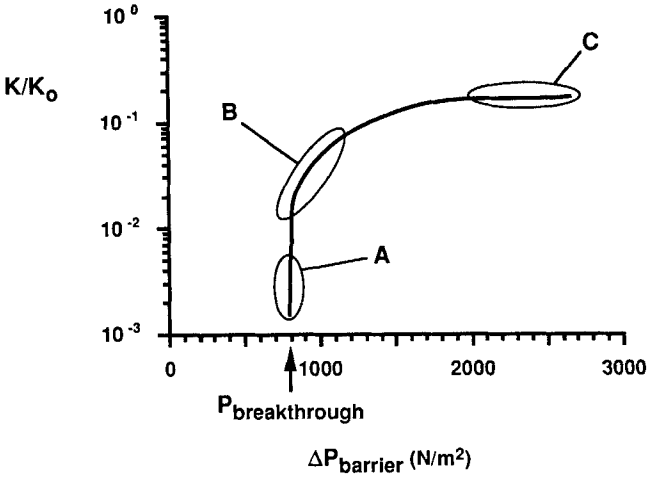

Figure 3. Foamed gel breakdown curve (Miller and Fogler, 1992).

Point A is the first conductive channel; region B, conductive network of channels grows; point C is the plateau permeability.

would be useful for studying the effect of parameters on foamed gel performance, especially under conditions that are difficult to achieve experimentally. A network model was used because it could account for the pore space heterogeneity inherent to porous media and can easily incorporate the complex pore level lens rupture phenomena responsible for conductive channel growth.

The presentation of the FGB model begins by reviewing existing breakdown models, followed by a description of the FGB model itself. The pore level phenomena on which the model is based are described, after which model results are presented. The problem under consideration is of importance to provide a fundamental understanding of the behavior of foamed gel barriers in porous media whose applications include conformance control in petroleum wells, contaminant containment in underground water flows, and subterranean storage of fluids.

Breakdown Models

Numerous model have been developed that simulate the transport properties or the breakdown of disordered media. These models can be categorized into three groups: (1) spring network models, which simulate the mechanical failure of materials (Sahimi, 1993; Sahimi and Goddard, 1985, 1986; Arbabi and Sahimi, 1990, 1993; Sahimi and Arbabi, 1992, 1993a,b; Curtin and Scher, 1990a,b; (2) electrical networks that simulate the change of network conductivity [electrical networks are claimed to be analogous to failure of disordered media (Kahng et al., 1988; de Arcangelis et al., 1989; Duxbury et al., 1987)]; and (3) percolation models, which represent spreading or transport in disordered media (Wilkinson and Willemsen, 1983; Chandler et al., 1982). Breakdown of these networks occurs when some fraction of the bonds that constitute the network "fail" after a prescribed threshold has been exceeded. For example, a resistor offers no resistance when a critical voltage drop is exceeded. Furthermore, the invasion percolation, the spring, and some of the electrical network models exhibit the threshold behavior that is desired: An

abrupt change in the network's macroscopic properties when a percolation cluster has formed.

Although the conductivity of a foamed gel barrier exhibits threshold behavior, there are subtle phenomenological differences between percolation in a foamed gel barrier and percolation exhibited by existing models. These differences prevent existing models from capturing the important aspects of foamed gel breakdown. Because the elastic lenses store energy *and* are anchored on a rigid lattice, the stress distribution in a network of uniform elastic lenses can diminish in a nonlinear manner from the point of the applied force. Neither spring nor resistor networks can exhibit a nonlinear stress distribution on a network with uniform properties because the nodes, or junctions where the springs join are "frictionless." The stress distribution has a dramatic effect on the type of network breakdown observed; the percolation behavior ranges from brittle failure (catastrophic growth of a single percolating cluster initiated by the failure of a single bond) for a uniform stress distribution to invasion percolation for a step function stress distribution. None of the existing models demonstrate a transition between brittle percolation and invasion percolation. Furthermore, it will be shown for the first time that the elastic modulus of the gel influences the stress distribution of the network.

The most closely related models are those developed specifically to study the minimum-path through networks that exhibit threshold conductivity (Roux et al., 1987; Rossen and Mamun, 1993; Sahimi, 1993). However, the elastic foamed gel breakdown resembles the minimal pathway model only for very low elastic modulus gels where the lenses strain uniformly along the entire length of the foamed gel barrier. In contrast, moderate and high elastic modulus gel lenses can store enough energy upon deformation that the pressure-induced strain dies out near the inlet face. The distinction between the two cases is the way the breakdown pressure increases with increasing network size. For an infinitely low elastic modulus (E) the breakthrough pressure gradient approaches a constant value as the network size approaches infinity, whereas for moderate E, the breakthrough pressure drop approaches a constant value when the network length exceeds the length of the pressure-induced lens strain region. Other notable differences between the foamed gel breakdown model and these minimal-path models are bonds that interact prior to rupture, and threshold values that depend upon the physical properties of the bond (lens). Instead of the commonly used on/off switch simulating an impermeable bond before rupture and a conductive bond after lens rupture, the bonds in the foamed gel breakdown model reflect the elastic deformation of the gelled lenses that displace and compress adjacent trapped gas bubbles. Any lens in contact with pressurized, displaced bubbles will also deform. This elastic behavior (a function of gel properties) is extremely important because it enables interior lenses to rupture first and allows many individually weak lenses to withstand a large applied force. This rupture of interior lenses first has not been previously modeled or experimentally observed. The bond threshold values and transport properties are based on experimental behavior of the gelled lenses. Thus, these networks are linked to the experimental breakdown phenomena, in contrast to other models (Roux et al., 1987; Rossen and Mamun, 1993; Sahimi, 1993).

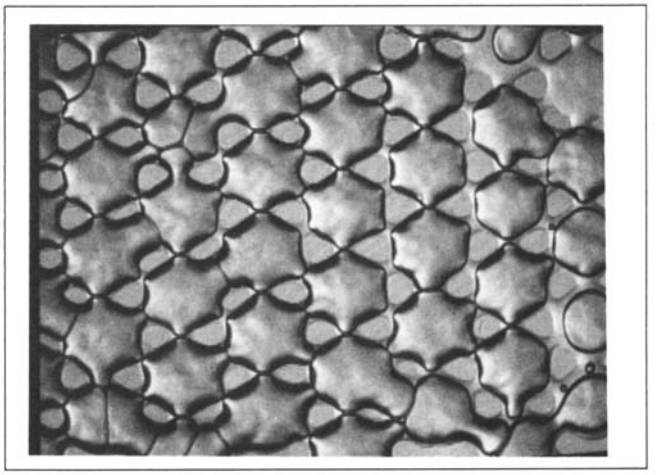

Figure 4. Foamed gel in an etched glass micromodel.

Description of the Foamed Gel Network Model

The translation of the foamed gel in porous media to a representative network is based upon the configuration of foamed gel in etched glass micromodels (Figure 4). The bonds and nodes of a network model represent the pore throats and pore bodies of porous media, respectively (Figure 5). Gelled lenses occupy the pore throats and gas bubbles reside in pore bodies. The gelled films that wet the micromodel pore body walls have a minor influence on breakdown and are therefore neglected in the network model.

The FGB model must be able to estimate the formation and evolution of conductive channels that control the permeability of the foamed gel barrier (Miller and Fogler, 1992). Pressure applied to one side of the foamed gel barrier ruptures channels and increases the barrier permeability. The breakdown rules formulated in the FGB model were supported by experimental observations; lenses (network bonds) are nonconductive prior to rupture and conductive after rupture. Although the lenses are nonconductive, they are "active" and influence the distribution of pressure throughout the network. A lens ruptures when the pressure drop across that lens exceeds a critical value.

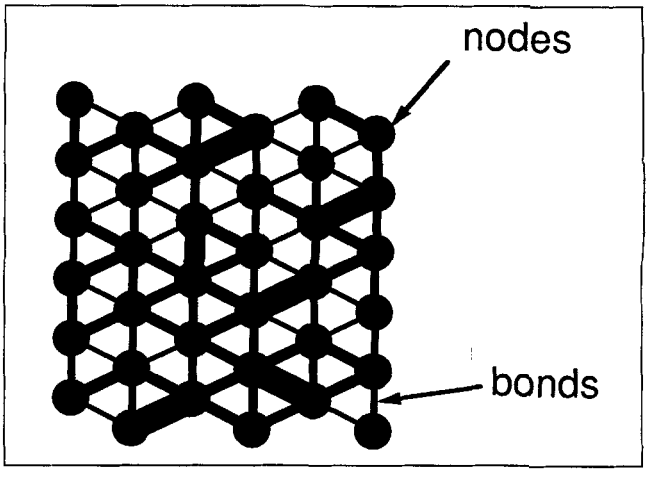

Figure 5. Model representation of pore space.

Characterization of the pore level foam structure is required to accurately simulate FGB. In addition to a broad range of lens sizes and strengths, defects in the form of bubbles that spanned multiple pore bodies were found in the foam structure during examination of foam in micromodels. Although the fraction of missing lenses, f, was small in our experiments, the individual defects were comprised of numerous missing lenses, that is, the missing lenses were in close spatial proximity. Duxbury et al. (1987) have shown that the largest defect governs the network strength; therefore, in contrast to previous models that randomly assign defects (Kahng et al., 1988; Sahimi and Arbabi, 1993b), the defects assigned to the FGB model network were *correlated defects* that represented the true nature of the large multipore spanning bubbles. Correlated defects were assigned to the network by randomly choosing a defect site and then performing a walk of N_s steps across the network and removing the lens at each step. The walk may be random (the case of a nonuniform defect distribution) or directed (the case of long defects oriented in one direction).

Pore Level Gelled Lens Behavior

The behavior of gelled lenses that span the pore throat has been considered on a more fundamental level to quantify the deformation of the lens and the pressure differential at which the lens fails. The lens behavior was described by simple expressions and experimentally determined relationships that were easily incorporated into the FGB model so the network bonds can emulate the real behavior of polymer gel lenses.

Lens deformation relationship

Gels commonly used in oil-field operations are water soluble polymers cross-linked with multivalent cations. Gel molecules stretched out of their low energy equilibrium state develop restoring forces to minimize polymer chain interactions with the solvent and other polymer chain segments (Shaw and Young, 1988). In an interacting network of gelled lenses, a fraction of the applied force will be balanced by the gel's restoring force, and the remainder will be transmitted to, and be balanced by, other lenses in the interior of the foam barrier. A simple model, described elsewhere (Miller, 1994), relates the lens strain, ϵ, to the applied pressure, the gel properties, and the dimensions of the lens,

$$\epsilon = \frac{L_2 - L_1}{L_1} = \frac{L_2}{2r_t} - 1 = \frac{(0.5)}{E}\frac{\Delta P \pi \ell_2}{V_{\text{gel}}}\left(\frac{\ell_2^2 + r_t^2}{2\ell_2}\right)^2, \quad (1)$$

where L_2 and L_1 ($L_1 = 2r_t$) are the strained lens silhouette perimeter length and the initial lens silhouette perimeter length, respectively; E is the elastic modulus; ℓ_2 is the axial deformation of the lens out of the pore throat; V_{gel} is the volume of gel in the lens; ΔP is the pressure differential across the lens; and r_t is the throat radius (see Figure 6). This equation reduces to the linear form shown in Eq. 2 when $\ell_2 \gg r_t$. It has been shown that a linear approximation of the lens deformation behavior can be used for all values of ℓ_2 in the network model with little loss of accuracy and great computational savings (Miller, 1994). The linearized lens deformation is

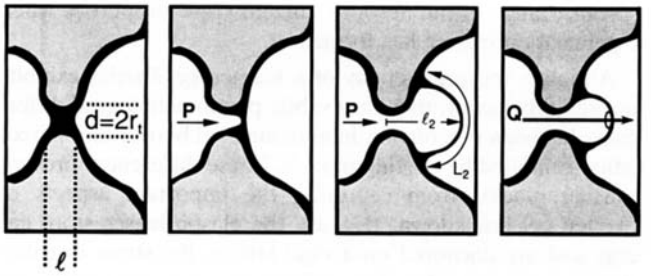

Figure 6. Lens in a capillary.

$$\epsilon = \frac{L_2 - L_1}{L_1} = \frac{(\ell_2 + r_t) - r_t}{r_t} = \frac{\ell_2}{r_t} = \frac{1}{C_{\text{lens}}}\Delta P. \quad (2)$$

The lens deformation constant, C_{lens}, which was found experimentally, is proportional to the linear elastic value of the elastic modulus, E. We found that the slope $1/C_{\text{lens}}$ scaled linearly with the ratio of the initial undeformed length of the lens and the constriction diameter (the lens aspect ratio, ℓ/d). For example, the deformation-constant relationship for the gel used in our previous study (1 wt. % polyacrylamide, 0.1 wt. % Cr[III] in deionized water) is

$$C_{\text{lens}} = \left(515 + 340\frac{\ell}{d}\right)^{-1} [\text{N/m}^2]. \quad (3)$$

Rupture pressure relationship

The gelled lens will rupture if the applied pressure exceeds the critical failure stress of the polymer network in the lens, σ^*. The lens rupture pressure, $P_{r\text{lens}}$, depends upon σ^* and the cross-sectional area on which σ^* acts. Because $P_{r\text{lens}}$ is a measure of the strength of an individual lens, it can be used as a simple criterion for lens rupture. The rupture pressure relationship is derived from a simplified force balance that relates the applied pressure to the stress in the gel-film that makes up the lens (Miller, 1994). At the rupture pressure, the force balance is written with respect to critical lens dimensions,

$$P_{r\text{lens}} = \frac{4t^*\sigma^*}{D_B^*}, \quad (4)$$

where t^*, D_B^*, and σ^*, are the critical film thickness, critical deformed lens diameter, and critical failure stress, respectively, at rupture. Using the conservation of gel volume, and assuming a form of t^* that scales with ℓ, $t^* = k\ell$, the rupture pressure becomes

$$P_{r\text{lens}} = \frac{k'\sigma^*\ell}{d} = A\left(\frac{\ell}{d}\right)^{\alpha}, \quad (5)$$

where k' is a constant, α is 1 for $t^* = k\ell$, and ℓ and d are the length of the unstrained lens and pore throat diameter, respectively; A (directly proportional to σ^*) and α were experimentally determined (Miller, 1994). The unstrained gelled

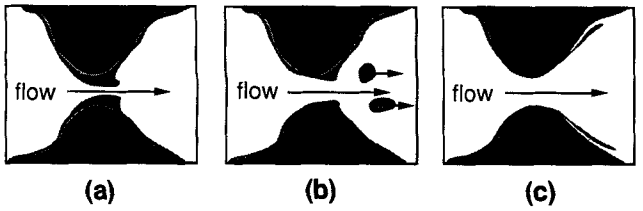

Figure 7. Three possible gel debris fates.

(a) Gel snap-back. (b) Gel break-off. (c) Gel stretching.

lens dimensions represent the initial condition of the foamed gel barrier and can be measured from microvisual experiments used to validate the model. For example, the rupture pressure relationship obtained for gas rupturing individual gelled lenses in a constricted capillary for 1 wt. % polyacrylamide with 0.1 wt. % Cr[III]·nitrate cross-linker, hereafter referred to as 1 wt. % HPA, is

$$P_{r\text{lens}} = 3{,}333\left(\frac{\ell}{d}\right)^{0.91} [\text{N/m}^2]. \tag{6}$$

Gel debris relationship

After the lenses rupture, fluid flow through conductive pores is restricted by gel debris that remains in or around the pore throats. The flow resistance due to gel debris is accounted for by a diameter reduction factor, R_f ($d_{\text{effective}}/d_{\text{initial}}$). An experimental relationship was sought to estimate R_f based upon the preruptured lens dimensions. However, because of the fate of the gel after lens rupture, the diameter reduction factor, R_f, varied significantly for identical lenses in experiments performed in capillary tubes with a single constriction. Figures 7a–7c shows three possible gel debris configurations (snap-back, break-off, and stretching) that produce different values of R_f. If all the gel snaps back into the pore throat, as shown in Figure 7a, it is expected that the resistance caused by the gel debris should scale with the amount of gel in the constriction and the constriction diameter. Alternatively, upon rupture the sudden rush of liquid flow through the constriction that follows lens rupture produces shear forces that can tear and remove gel fragments or cause the gel to peel off the constriction wall (see Figure 7b). It was also observed that the gelled lens often became pressed along the pore body wall as it deformed prior to rupture; after rupture, fluid flow was virtually unimpeded by gel debris because it was stuck to the pore body wall (see Figure 7c).Whether gel sticks to a pore wall is an unknown function of the affinity of the gel to whatever coats the wall, the magnitude of the elastic restoring force, and the contact area between the film and the wall.

The experimental results showed that R_f was small when the debris snapped back into the pore throat ($R_f < 0.3$) and large otherwise ($R_f > 0.7$). However, the fate of the gel after lens rupture was inherently unpredictable and no simple scaling relationship between R_f and ℓ/d was apparent based on these experiments. In the absence of a gel debris relationship the FGB model will be used to assess the average value of R_f for several different foamed gel barriers.

Results and Discussion

The primary goals of this work are to predict the FGB curve and to study the FGB process. The analysis of FGB will focus on the evolution of network permeability and the conductive channels with increasing pressure.

FGB was simulated with a triangular, two-dimensional network that was the same as the pore space of micromodels used in experiments. The algorithm listed below describes how to apply the FGB model to the micromodel experiments.

(1) Decorate the network with pore throats, lenses, and defects.

(2) Apply a pressure differential to the network. Lenses strain due to the pressure differential and cause a volumetric change in adjacent bubbles. It is assumed the bubbles are ideally compressible, and therefore, bubble pressures are estimated with the following equation,

$$P_i = \frac{P_{oi}^* V_{oi}}{V_{oi} - \Sigma \Delta V_j},$$

where P_i is the pressure of the ith bubble, P_{oi} and V_{oi} are the original pressure and volume of that bubble, and ΔV_j are the individual bubble volume changes due to deformation of lenses surrounding bubble "i".

(3) If the pressure drop across a lens exceeds its rupture pressure, P_r (determined from experimental relationship), the lens will rupture.

(4) If multiple lenses are eligible for rupture at a given pressure, the lens with the greatest rupture potential ($[\Delta P_{\text{lens}} - P_{r\text{lens}}]/P_{r\text{lens}}$) ruptures first.

(5) If a lens between separate gas bubbles ruptures, the gas mixes and is treated as one bubble that spans both pore bodies.

(6) If a ruptured channel percolates the network, fluid flow through the pore throats is governed by the Hagen–Poiseuille equation. The post rupture pore throat diameter is constricted by ruptured gel debris.

(7) If no additional lenses rupture, increase the inlet pressure and go to step 3.

Etched glass micromodels, manufactured from two glass plates with an interconnected network of channels etched into their surface, were used to visualize foamed gel breakdown in porous media and have been described elsewhere (Miller and Fogler, 1992). The micromodels allow one to observe the formation of conductive channels as well as determine the evolution of permeability as the foamed gel breaks down. Previous studies have shown that foamed gel breakdown in micromodels emulates the breakdown phenomena in consolidated porous cores (Miller, 1994). Comparison of experiment and predicted breakthrough pathways and breakdown curves form the basis of the model verification.

Prediction of the first breakthrough pathway

Pathway prediction is important because it indicates that the mechanics of FGB are properly accounted for in the network model. Furthermore, the model must predict the location of ruptured channels so that it can be used to estimate foamed gel performance in macroscopically heterogeneous media. The predicted breakthrough pathways were compared

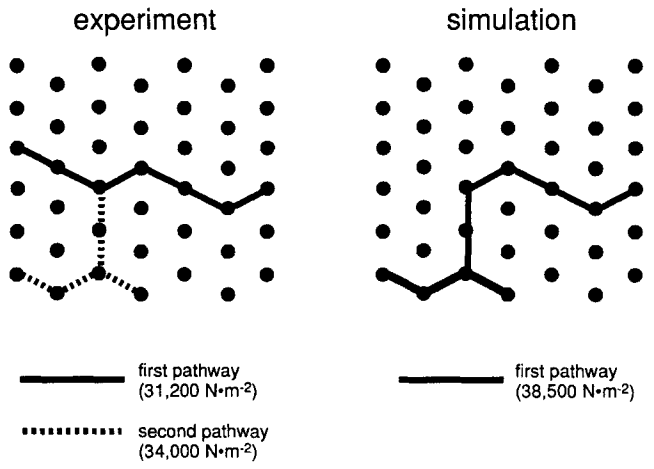

Figure 8. Actual vs. predicted breakthrough pathways.

with breakthrough pathways that ruptured through foamed gel barriers in micromodel experiments. The breakthrough pathway and barrier rupture pressure were recorded during each experiment. The lengths and diameters of the gelled lenses were measured from video images and input into the same "location" in the FGB model. This one-to-one mapping of gelled lens dimensions from the experiment to the model accounted for all foam defects and any other microscopic heterogeneities that were present in each of the experiments.

The results of a typical experiment and the corresponding theoretical predictions of the flowpaths is shown in Figure 8. In this experiment, the rupture of the first breakthrough pathway, formed at 31,200 $N \cdot m^{-2}$, supported an extremely small flow rate. A second, highly conductive pathway suddenly formed at 34,000 $N \cdot m^{-2}$. The foamed gel model predicted this high conductivity channel as the first conductive channel. The predicted rupture pressure of 38,500 $N \cdot m^{-2}$ was found by using the experimentally obtained relationships discussed previously and without adjusting any parameters. This result compares very favorably with the experimental value for the highly conductive channel.

Numerous other breakthrough pathway experiments were carried out and several representative results are shown in Figure 9. Overall one observes there is very good agreement between the model predictions and the experimental results. The few discrepancies that were observed (such as experiment 5 in Figure 9) may be attributed to two factors: (1) lenses whose rupture pressure, P_{rlens}, deviates from the rupture pressure relationship, and (2) uncertainty in the measurement of the lens aspect ratios that results in inaccurate rupture pressures. The P_{rlens} can deviate from values predicted from Eq. 6 due to undetectable defects in the gelled lenses (Miller, 1994; Barteneve and Zuyev, 1968). These microscopic defects cause a group of apparently identical lenses to have a distribution of rupture pressures. The measurement errors originate from measuring the two-dimensional lens silhouette dimensions (ℓ and d) from a recorded image on a video monitor. Because the rupture pressure relationship is very sensitive to lens dimensions, the rupture pressure estimates can be in error by as much as 15%. In spite of these two limitations, the agreement between the model and experiment indicates that lens deformation and rupture adequately represents the FGB mechanism.

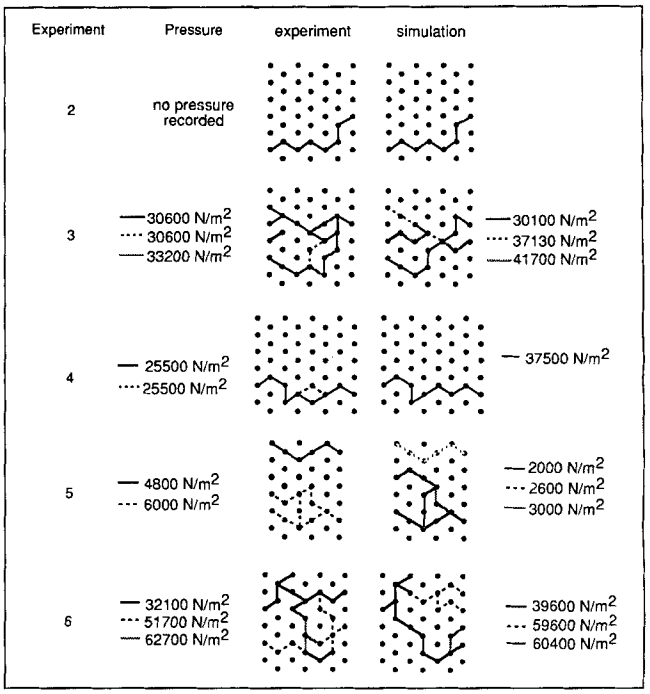

Figure 9. Experimental vs. simulated rupture pathways.

Effect of elasticity on breakthrough

A comparison of the lens rupture sequence between a low and a high elastic modulus foamed gel illustrates the role of lens deformation on the breakdown process. Figures 10a–10d and 11a–11d illustrate the growth of conductive pathways in a system of interacting and noninteracting (rigid) lenses, respectively. The stick figures are the model representation of the foam in porous media. The numbers on the stick figures indicate the strength of the lens (1 is the weakest). The illustrations beneath the stick figures are foam in porous media; lenses are lines and porous media grains are the irregular shapes. The thick lines in the stick figures are ruptured lenses, and the lighter-shade lines are lenses that are close to rupture. The applied pressure is transmitted throughout the elastic foam barrier (Figure 10a), whereas the applied pressure is only felt by lenses along the interface of the invading fluid in the rigid foam barrier. The pressure distribution through the elastic lens network has two effects on breakdown. First, and most importantly, interior lenses can rupture first (Figure 10b). Interior lenses are not in direct contact with the inlet face or a channel that originates from the inlet face. Second, many individually weak lenses can withstand a large macroscopic pressure gradient. As a consequence of the second effect, the barrier rupture pressure will greatly exceed the rupture pressure of any individual lens in the breakthrough cluster. The rupture of a single elastic lens within the strained elastic barrier can set off a lens rupture chain reaction, creating a conductive channel that percolates the network without further increases of pressure (Figures 10c–10d). In contrast, the rigid barrier's breakthrough pathway must originate at the inlet face (Figure 11b) and advances only if the injection pressure exceeds the strength of the weakest bond on the interface.

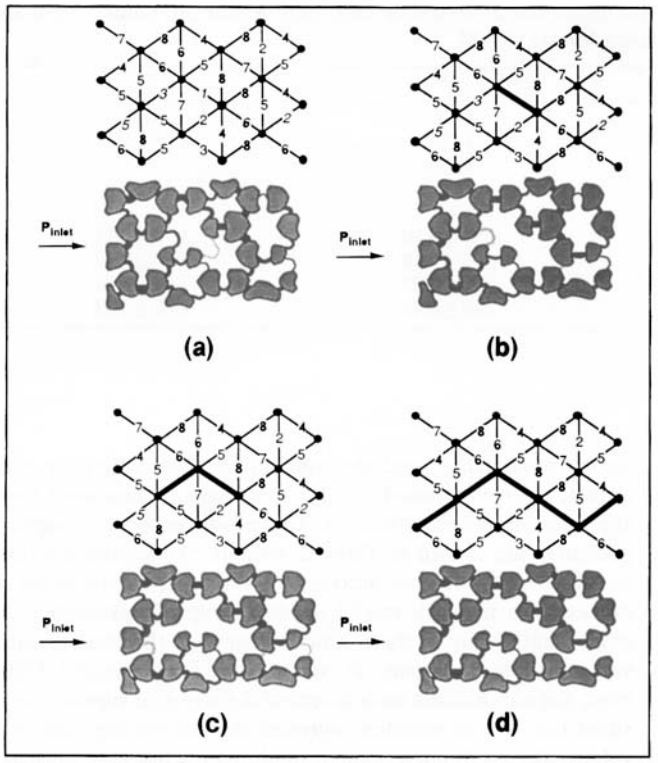

Figure 10. (a) Lens deformation in an elastic foamed gel barrier; (b) lens rupture chain reaction is initiated by interior lens rupture; (c) ruptured lens cluster growth in an elastic foamed gel barrier; (d) a conductive channel percolates the network.

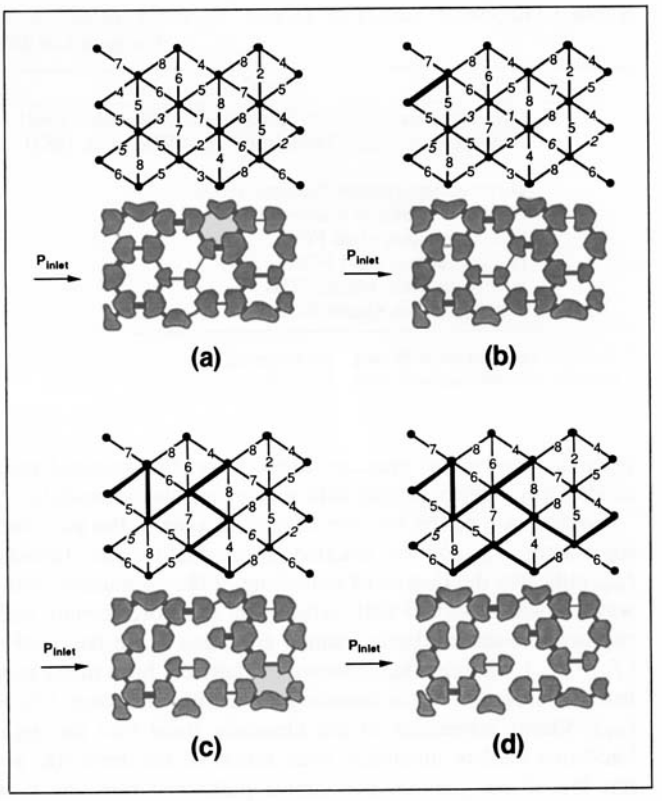

Figure 11. (a) Pressure is not transmitted into the interior of a rigid foamed gel; (b) weakest lens along the inlet face must rupture first; (c) ruptured lens cluster growth in a rigid foamed gel barrier; (d) a conductive channel percolates the network.

Characterization of breakthrough pathway structure

The topography of a percolating cluster is characterized by (1) determining the number of ruptured lenses in the first conductive pathway (the breakthrough cluster), N and (2) determining the number of the ruptured lenses through which fluid flows (the conducting backbone of the breakthrough cluster), N_b. The size of conductive clusters and the size of the conducting backbone scale with the network dimensions as shown below:

$$\frac{N}{N_{\text{total}}} = f_N \propto L^{D-2} \tag{7}$$

$$\frac{N_b}{N_{\text{total}}} = f_{N_b} \propto L^{D_b-2}, \tag{8}$$

where N_{total} is the total number of pore throats in the network, f_N is the fraction of the total lenses that make up the percolating cluster, f_{Nb} is the fraction of the total lenses that make up the conductive backbone, and the 2 in the exponent is the network dimension. Because the size of these clusters scales with network size according to the apparent exponents D and D_b in the preceding equations, the clusters are said to be fractal in nature. The two apparent fractal dimensions, D, the apparent fractal dimension of the percolating cluster, and D_b, the apparent fractal dimension of the conducting backbone, are estimated for both elastic and rigid foamed gel barriers using network sizes ranging from 5×5 to 38×38 (summarized in Table 1 for both heterogeneous and homogeneous networks).

A comparison of the rigid and elastic foamed gel apparent fractal dimensions with accepted fractal dimensions for other models relates this model to others. Fractal dimensions of other breakdown models are also summarized in Table 1. The dimension, D, for a rigid foamed gel cluster is similar to that of invasion percolation, whereas D for elastic foamed gel breakdown is approximately the same as the minimal pathway fractal dimension. Because the apparent fractal dimension of rigid foamed gel is the same as invasion percolation (the problems are formally identical), one expects rigid foamed gel to follow the same behavior that has been documented in the literature for invasion percolation in two- and three-dimensional lattices. The behavior of interest includes the scaling of the conductive network of channels in three dimensions and the network conductivity above the percolation threshold. Information regarding elastic FGB that may be gained from minimal pathway models includes theoretical expressions (although for different lattices) for the macroscopic gradient at which a conductive channel first appears (Rossen and Mamun, 1993). Additionally, minimal pathway models suggest there is a region near the barrier rupture pressure where there is a power law dependence of network

Table 1. Reported Values of D and D_b for Percolation in Two-Dimensional Networks and New Apparent Values from the Foamed Gel Breakdown Model (FGB)

Model	D	D_b
Ordinary percolation (Wilkinson and Willemsen, 1983)	1.89	1.64
Invasion percolation (Wilkinson and Willemsen, 1983)	1.89*	1.64
	1.82†	
Directed percolation (Sahimi, 1993)	1.34	1.18
Minimum pathway (Sahimi, 1993)	1.13	
Heterogeneous, rigid FGB	1.84 ± 0.10	1.70 ± 0.11
Homogeneous, rigid FGB	1.92 ± 0.10	1.64 ± 0.10
Heterogeneous, elastic FGB	1.06 ± 0.04	1.00 ± 0.05
Homogeneous, elastic FGB	1.02 ± 0.03	1.00 ± 0.03

* Invasion percolation without phase trapping.
† Invasion percolation with phase trapping.

permeability on the pressure drop. Note, the minimal path model only applies to gels with a very low elastic modulus.

Comparison of the fraction of pore throats in the percolating cluster, f_N, and the fraction of conductive pore throats, f_{Nb}, indicates the degree of branching of the conductive pathways. It was observed that virtually all the pore throats with ruptured lenses in elastic foamed gel barriers are conductive ($f_N = f_{Nb}$), whereas rigid foamed gel barriers have many ruptured lenses that form nonconductive side branches ($f_N > f_{Nb}$). Visual inspection of the channels show that the rigid backbone cluster meanders over much of the network, yet has few if any parallel conductive pathways; thus the flow path through foamed gel barriers with a high elastic modulus is in general much longer and more tortuous than the elastic foamed gel conductive backbone.

Prediction of the FGB curve

The FGB model was further tested by comparing simulated FGB curves with FGB curves obtained from micromodel experiments (micromodel pore space contained 3,600 pore bodies and 10,800 pore throats). In these experiments, several hundred lens lengths and pore throat diameters in a micromodel were measured, and the resulting size distributions were introduced into the model. The foamed gel model networks were decorated by randomly sampling lens and pore throat size distributions measured from the experiments and then invoking the aforementioned correlated defect decoration procedure (directed defects were used). The fraction of lenses removed, f, and the number of steps taken for each defect, N_s, were based on the same values measured from the micromodel experiments. The predicted barrier rupture pressures are shown in Table 2, column "P_r Simulation [Defects]." If one does not account for the spatial correlation of defects, the network model produces rupture pressure estimates that are up to three times larger than the experimental values (Table 2 column "P_r Simulation [No Defects]"). However, the simulations with directed defects give rupture pressures that are in excellent agreement with the experimental values. The FGB curve from a random network with uncorrelated defects is compared to that from a random network with directed defects in Figure 12. In addition to a lower barrier rupture pressure, P_r, the correlated defect simulations had a marginally quicker permeability increase with pressure.

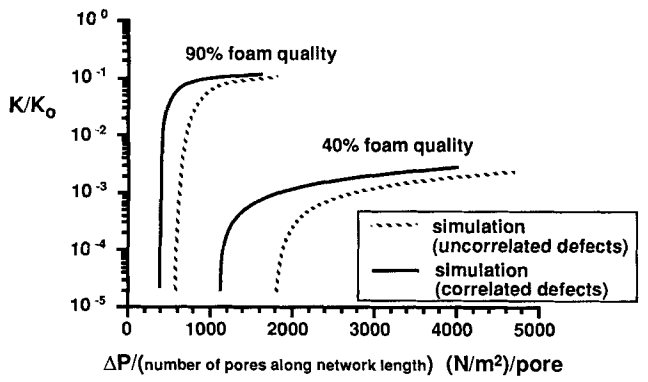

Figure 12. Effect of correlated defects on foamed gel breakdown curves.

Simulations were run using ten network decorations for each experiment with the average breakdown curve compared to the experimental breakdown curves. The gel debris constriction factor, R_f ($d_{\text{effective}}/d_{\text{initial}}$) was matched to the plateau permeability; all other parameters were determined experimentally. Two foamed gel barriers with different foam quality (identical gel composition) and three foamed gel barriers with different gel composition (the same foam quality) were used in the comparison. The experiment and simulated FGB curves are shown in Figures 13 and 14 for constant gel composition and constant foam quality, respectively. The 90% foam quality, 1% HPA gel foamed gel experiment and simulation shown in Figure 13 represents a special case that will be discussed later. Table 2 summarizes the values of R_f that correspond to the plateau permeabilities. The effective resistance factor, R_f, decreased (that is, the resistance increased) as the foam quality decreased and the gel strength increased.

Table 2. Summary of Parameter Values Used in Foamed Gel Breakdown Curve Comparison with Experiment

Foamed Gel Barrier			P_r Simulation (No Defects)	P_r Simulation (Defects)	P_r Experiment
wt. % HPA	vol. % Gas	Avg. R_f	(N/m²)	(N/m²)	(N/m²)
1.0	40	0.02	$1,820 \pm 89$	$1,104 \pm 99$	1,193
1.0	80	0.1	$1,560 \pm 87$	950 ± 80	880
1.0	90	0.16	580 ± 38	245 ± 25	282
0.5	90	0.36	370 ± 19	80 ± 8	122
2.0	90	0.04	$6,360 \pm 410$	$3,170 \pm 254$	1,150

* The error reported for the P_r values is one standard deviation.

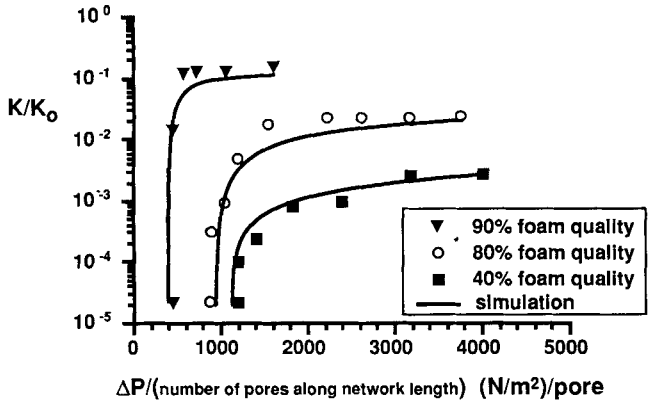

Figure 13. Model predictions vs. experimental results for three foamed gel barriers of different foam quality.

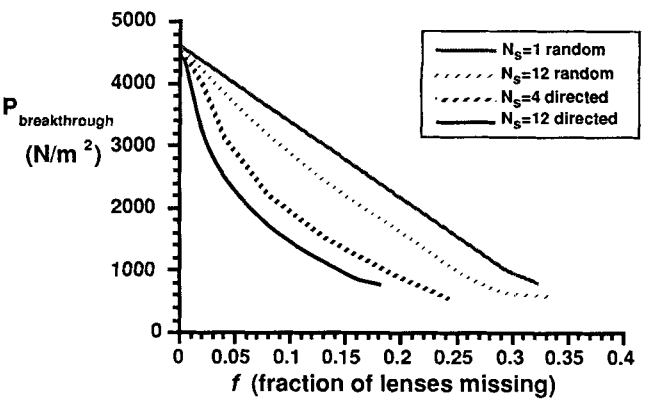

Figure 15. Effect of defects on the barrier rupture pressure of a 20×20 network.

These trends should be expected because flowpaths are more constricted (smaller R_f) for greater volumes of gel in the pore space, and strong gels are less susceptible to shear forces that erode the constricting gel in the pore throat.

A final comparison of the predicted FGB curve was made with an independent experiment in which R_f was not matched to the plateau permeability. In this experiment a 90% quality foamed gel barrier was created from a 1 wt. % HPA gel (Figure 13). The value of R_f from Table 2 was used and no parameters were adjusted. There was good agreement between the experimental and the predicted foamed gel breakdown curves.

Parameter analysis

The FGB model has been shown to provide an adequate estimate of the performance of foamed gel barriers in a representative porous medium. Hence the model will be used the explore the effect of parameters that influence FGB. The parameters studied are categorized into two groups: (1) microscopic heterogeneity of the foamed gel structure, and (2) physical properties of the gel. The number of correlated defects, the standard deviation of the pore throat size distribution, s_{pt}, and the standard deviation of the lens length distribution, s_ℓ, were varied to investigate the effect of microscopic heterogeneities on foamed gel breakdown. The critical failure stress σ^*, and the elastic modulus, E, were varied to study the effect of gel properties. These parameters influence the barrier rupture pressure and the slope of the ascending portion (region B on Figure 3) of the breakdown curves. All of the simulations used networks with 100% of the pores accessible to gas. Therefore, the plateau permeability only depends on the number and the location of intact lenses and the gel debris constriction factor (held constant for all runs). Except where noted otherwise, the lens deformation constant and lens rupture pressure correlations were Eqs. 6 and 3, respectively (linear strain region E is approximately 130 N/m^2), and the gelled lens aspect ratios were normally distributed about a mean of 1.0 with a standard deviation of 0.33.

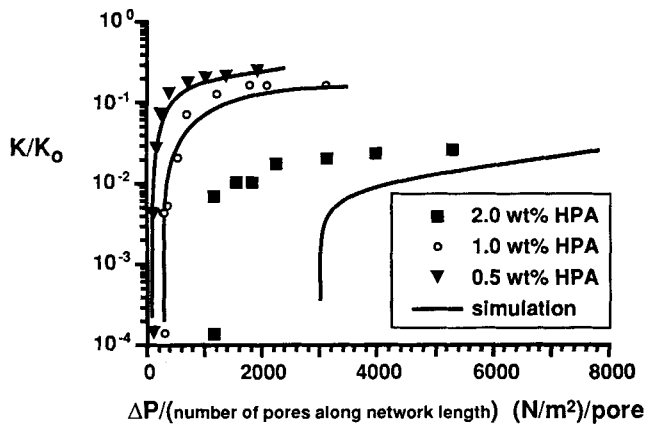

Figure 14. Experimental vs. predicted foamed gel breakdown curves for three different polymer concentrations.

Correlated defects

A small fraction of missing lenses can significantly reduce the foam gel barrier rupture pressure, P_r, when the missing lenses group together to make a small number of large defects. Figure 15 shows how the barrier rupture pressure decreases with the fraction of missing lenses for several different defect sizes (number of missing lenses in a single defect). The defect size was controlled by performing a random walk or a directed walk of a specified number of steps, N_s. Random walk defects meander in any direction, whereas directed walk defects only extend in the direction of the macroscopic pressure gradient. The presence of random walk correlated defects decreased the barrier rupture pressure to a greater extent than uncorrelated defects. Furthermore, the magnitude of the decrease in rupture pressure was higher for defects created from larger random walks that represent a strong spatial correlation of defects. The P_r reduction was most significant for directed walk defects on networks with small missing lens fractions. For example, P_r was reduced by 40% in a network with only 3% of its lenses missing in the form of 12-step directed walk defects, whereas the P_r reduction was only 12% and 5% for 12-step random walk defects and uncorrelated defects, respectively (20×20 network was used). The experiments showed that on average, the fraction of missing lenses and the number of missing lenses per directed defect were about 0.04 and 8, respectively. The directed walk defects have a longer projected length parallel to the pres-

sure gradient than random walk or uncorrelated defects, and it is the projected length of the defect that dominates the reduction in rupture pressure (Duxbury et al., 1987). Because the defect type had a strong influence on the network failure stress, one must decorate the FGB model with the appropriate defect type. Random uncorrelated defects represent well-mixed composite systems, random walk defects resemble poorly mixed composites, and directed walk defects represent defects in composite systems where flow conditions orient reinforcement fibers, and of course, the case of foamed gel barriers studied here.

Microscopic Heterogeneity. Microscopic heterogeneity of the porous media influences the lens aspect ratio (ℓ/d) and consequently influences the distribution of lens rupture pressures and deformation constants. A heterogeneous lens system will have a nonuniform stress distribution that gives rise to transverse pressure gradients that are absent in a uniform lens system. Because uniform foamed gel has no transverse pressure gradients, ruptured lens channels will only grow in length toward the inlet and exit faces. As microscopic heterogeneity increases, transverse pressure gradients develop locally that can cause lens rupture and channel growth to occur perpendicular to the macroscopic pressure gradient. Microscopic heterogeneity was introduced in two different ways:

(1) Uniform lens lengths were assigned to networks decorated with a distribution of pore throat diameters. A mean pore throat diameter of 1×10^{-4} m was used in every run, and S_{pt} was varied from 3×10^{-6} to 1×10^{-4}m.

(2) A distribution of lens lengths was assigned to networks decorated with a uniform pore throat diameter. A mean lens length of 1×10^{-4} m was used in every run, and s_ℓ was varied from 3×10^{-6} to 1×10^{-4} m.

The effect of the lens length and the pore throat diameter distributions are shown in Figures 16a and 16b, respectively. In both cases, foamed gel with little microscopic heterogeneity (small value of s_{pt} or s_ℓ) had a high barrier rupture pressure and very straight, narrow percolating channels. The barrier rupture pressure is highest for uniform foam because there are no weaknesses or defects that will prematurely initiate the lens rupture chain reaction discussed previously. It was also observed that a uniform foamed gel barrier's permeability increased from zero to the plateau permeability over a small range of injection pressures. The sharp rise in network permeability was a result of the simultaneous rupture of many similar strength lenses in the uniform foamed gel. Breakthrough channel formation in heterogeneous foamed gel began with the weakest pathway (Rossen and Mamun, 1993; Sahimi, 1993; Kahng et al., 1988); thus, the pressure must increase before the remaining, stronger lenses rupture. The permeability increase that accompanies channel formation in heterogeneous foamed gel barriers depends upon how the heterogeneity was introduced. When a uniform pore throat diameter was used, heterogeneity comes from the distribution of the length of the lenses. As can be seen in Figure 16a, the permeability increased to the same plateau permeability in all cases, but required a larger range of pressure than that for uniform foams. On the other hand, when the lenses are uniform and the pore throat diameters are heterogeneous, the breakthrough cluster will form through the largest pore throats. The resulting conductive flow channels will be highly conductive and the permeability will rise rapidly, as shown in

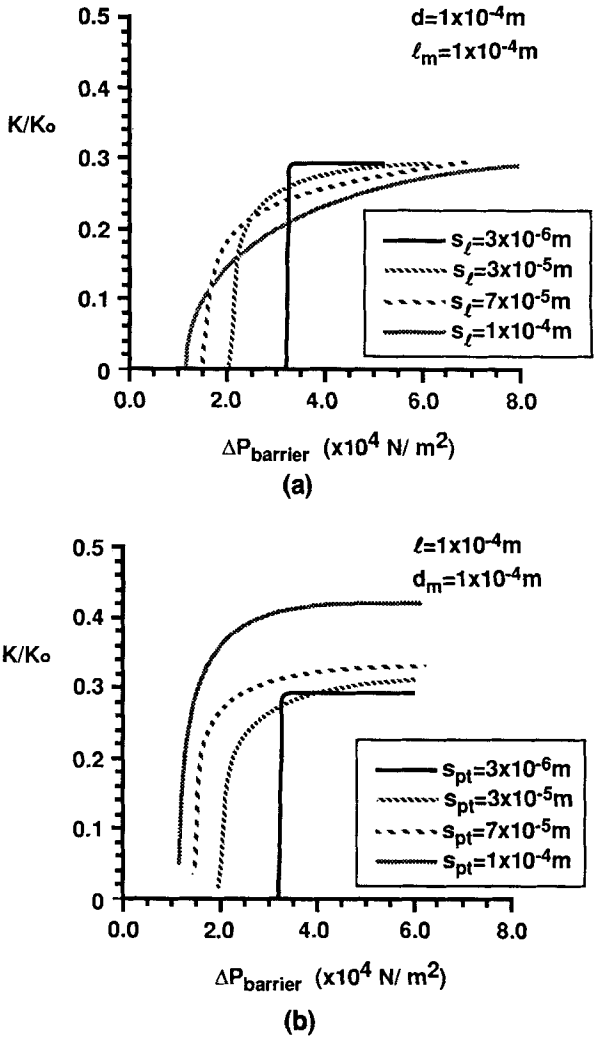

Figure 16. Effect of pore throat heterogeneity on foamed gel breakdown.

S_{pt} and s_ℓ are the standard deviation of the pore throats and lens lengths, respectively.

Figure 16b. Furthermore, the conductivity of these heterogeneous networks were higher than the uniform barrier with the same mean diameter size; thus the plateau permeability increased with heterogeneity.

Gel Physical Properties. The gel critical failure stress, σ^*, increases with polymer and cross-linker concentration for water-soluble polymer gels, and is a measure of the gel's ability to resist rupture. The constant, A, in the rupture pressure relationship (Eq. 5) is proportional to σ^* and therefore, the barrier rupture pressure scales with σ^*. The rate of permeability increase with pressure is inversely proportional to σ^*.

The elastic modulus, E, controls the deformation of gelled lenses, which influences the stress distribution throughout the foamed gel barrier. When a lens is deformed, it displaces trapped gas bubbles and it is the displaced bubble that exerts force upon and deforms adjacent, interior lenses. The volume of gas displaced due to gelled lens deformation (and the accompanying stress distribution to adjacent lenses) is inversely dependent upon E. The stress distribution across the foamed gel barrier ranges from uniform to highly nonuniform (for

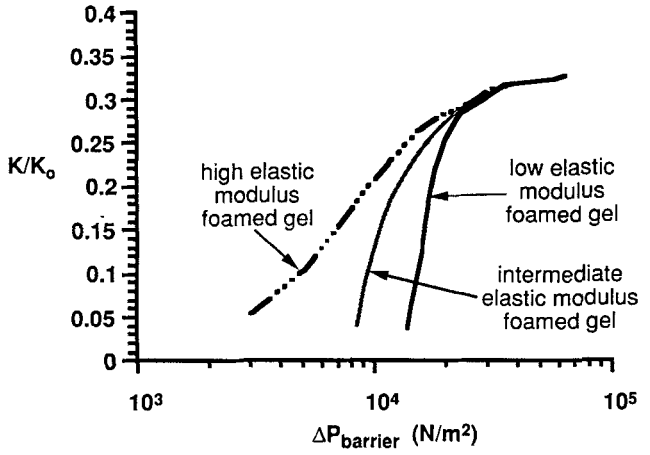

Figure 17. Effect of the elastic modulus on foamed gel breakdown.

example, only lenses at the interface between the barrier and the injected fluid are under stress) depending on the elastic modulus. Figure 17 shows three foamed gel breakdown curves that represent a broad range of elastic modulus values. It is evident that the foamed gel barrier rupture pressure and rate of permeability increase decrease as the gel elastic modulus increases.

Summary and Conclusions

Foamed gel barriers efficiently render porous media impermeable to gas or liquid flow. However, exceeding a critical pressure drop across the barrier will rupture lenses and form conductive channels. It is important to know the maximum pressure a given barrier can withstand and the evolution of the barrier permeability during breakdown. An FGB model has been developed that gives results consistent with laboratory experiments. When used in conjunction with other models or experiments that indicate foam placement in a macroscopically heterogeneous system, the current model can provide an estimate of the performance of a linear foamed gel profile modification treatment. This FGB model also exhibited interesting breakdown characteristics, which are summarized below:

(1) Breakthrough and breakdown simulated with the FGB model have a unique dependency on the elastic modulus of the gel. Increasing the gel's elastic modulus causes the breakdown behavior to change from what is called "brittle fracture" for low elastic modulus (soft) gels, to invasion percolation for high elastic modulus (rigid) gels. This wide range in the breakdown behavior can occur regardless of the microscopic structural heterogeneity of the foamed gel barrier. Other models that exhibit a wide range of breakdown behavior only do so when there is sufficient microscopic heterogeneity in the form of weak or missing network elements.

(2) The elastic modulus influences the deformation of the lenses and thus influences their interaction with other lenses. It is the change in the deformation (interaction) of lenses with the elastic modulus that causes the breakdown to change character. Rigid, noninteracting lenses fail independently when the applied pressure exceeds that lens's rupture pressure. Furthermore, only lenses along the interface between the injected fluid and the foamed gel barrier feel the applied pressure. Elastic lenses deform and interact to cooperatively withstand applied pressure and therefore a series of individually weak lenses can withstand a large pressure differential that is much greater than the rupture pressure of any of the individual lenses. Furthermore, because all the interacting lenses are strained, weak interior lenses can rupture first.

(3) The FGB model shows that breakdown is adequately represented by the breakdown of a system of interacting gelled lenses. The evolution of the predicted FGB pathways agrees with experimental observations.

(4) Defects in the form of elongated bubbles that span many pore bodies in foamed gel barriers reduce the barrier rupture pressure. To accurately estimate the rupture pressure the model networks were decorated with spatially correlated defects that resemble the elongated bubbles. It was important to decorate the network with defects that resemble the elongated bubbles because a small fraction of missing lenses can significantly reduce the barrier rupture pressure when the missing lenses group together make a small number of large defects (as was the case with the elongated bubbles). Model networks with randomly distributed, uncorrelated defects (missing lenses) overestimated the barrier rupture pressure.

Notation

K = permeability, m^2
K_o = pretreatment permeability, m^2
K/K_o = posttreatment permeability ratio
ℓ_m = mean lens length
n = moles of gas in a cluster
P_c = fraction of lenses ruptured at breakthrough
R_g = universal gas constant, $kg \cdot m^2 \cdot s^{-2} \cdot mol^{-1} \cdot K$
T = temperature, K

Literature Cited

Ali, L., *Dynamic Behavior of Soils Partially Grouted by a Foaming Process*, PhD Thesis, The Univ. of Michigan, Ann Arbor (1992).

Arbabi, S., and M. Sahimi, "Test of Universality for Three-Dimensional Models of Mechanical Breakdown in Disordered Solids," *Phys. Rev. B*, **41**(1), 772 (1990).

Arbabi, S., and M. Sahimi, "Mechanics of Disordered Solids. I. Percolation on Elastic Networks with Bond Bending Forces," *Phys. Rev. B*, **47**(2), 695 (1993).

Barteneve, G. M., and Y. S. Zuyev, *Strength and Failure of Visco-Elastic Materials*, Pergamon Press, New York (1968).

Benge, O. G., L. B. Spangle, and C. W. Sauer, "Foamed Cement-Solving Old Problems with a New Technique," SPE 11204, Fall Technical Conf. and Exhib., New Orleans, LA (Sept. 26–29, 1982).

Chandler, R., J. Koplic, K. Lerman, and J. F. Willemsen, "Capillary Displacement and Percolation in Porous Media," *J. Fluid Mech.*, **119**, 249 (1982).

Chmilowski, W., and L. B. Kondratoff, "Foamed Cement for Squeeze Cementing Low-Pressure, Highly Permeable Reservoirs: Design and Evaluation," *SPE Drilling Eng.*, 284 (1992).

Clampitt, R. L., "Formable Compositions and Formation Treatment," U.S. Patent 4,300,634 (Nov. 17, 1981).

Curtin, W. A., and H. Scher, "Brittle Fracture in Disordered Materials: A Spring Network Model," *J. Mat. Res.*, **5**(3), 535 (1990a).

Curtin, W. A., and H. Scher, "Mechanics Modeling Using a Spring Network," *J. Mat. Res.*, **5**(3), 554 (1990b).

de Arcangelis, L., A. Hansen, H. J. Herrman, and S. Roux, "Scaling Laws in Fracture," *Phys. Rev. B.*, **40**(1), 877 (1989).

deRozieres, J., and R. F. Ferriere, "Foamed Cement Characterization Under Downhole Conditions and Its Impact on Job Design," *SPE Prod. Eng.*, 297 (1991).

Douben, D. L., "Increasing Foam Stability in Earth Formations," U.S. Patent 3,530,940 (Sept. 20, 1970).

Duxbury, P. M., P. L. Leath, and P. D. Beale, "Breakdown Properties of Quenched Random Systems: The Random-Fuse Network," *Phys. Rev. B.*, **36**(1), 367 (1987).
Ettinger, R. A., and C. J. Radke, "Influence of Foam Texture on Steady Foam Flow in Berea Sandstone," *SPE Res. Eng.*, **7**(1), 83 (1992).
Hazlett, R. D., and P. Shu, "Amino Resin Modified Xanthan Polymer Foamed with a Chemical Blowing Agent," U.S. Patent 4,830,108 (May 16, 1989).
Kahng, B., G. G. Batrouni, S. Redner, L. de Arcangelis, and H. J. Herrmann, "Electrical Breakdown in a Fuse Network with Random, Continuously Distributed Breaking Strengths," *Phys. Rev. B*, **37**(13), 7625 (1988).
Miller, M. J., "Permeability of Foamed Gel Barriers Used for Physical Control of Subterranean Fluid Movement," PhD Diss., The Univ. of Michigan, Ann Arbor (1994).
Miller, M. J., and H. S. Fogler, "A Mechanistic Investigation of Waterflood Diversion Using Foamed Gels," SPE 24662, Technical Conf. and Exhib. of the SPE, Washington, DC (Oct. 4–7, 1992).
Oertel, G., ed., *Polyurethane Handbook*, Hanser, New York (1985).
Rossen, W. R., and C. K. Mamun, "Minimal Path for Transport in Networks," *Phys. Rev. B*, **47**(18), 11815 (1993).
Roux, S., A. Hansen, and E. Guyon, "Criticality in Non-Linear Transport Properties of Heterogeneous Materials," *J. Phys.*, **48**, 2125 (Dec. 1987).
Sahimi, M., "Nonlinear Transport Processes in Disordered Media," *AIChE J.*, **39**(3), 369 (1993).
Sahimi, M., and J. D. Goddard, "Elastic Percolation Models for Cohesive Mechanical Failure in Heterogeneous Systems," *Phy. Rev. B*, **33**(11), 7848 (1986).
Sahimi, M., and J. D. Goddard, "Superelastic Percolation Networks and the Viscosity of Gels," *Phys. Rev. B*, **32**(3), 1869 (Aug. 1985).
Sahimi, M., and S. Arbabi, "Percolation and Fracture in Disordered Solids and Granular Media: Approach to a Fixed Point," *Phy. Rev. Lett.*, **68**(5), 608 (Feb. 1992).
Sahimi, M. and S. Arbabi, "Mechanics of Disordered Solids. II. Percolation on Elastic Networks with Central Forces," *Phys. Rev. B*, **47**(2), 703 (Jan. 1993a).
Sahimi, M., and S. Arbabi, "Mechanics of Disordered Solids. III. Fracture Properties" *Phys. Rev. B*, **47**(2), 713 (Jan. 1993b).
Shaw, M. C., and E. Young, "Rubber Elasticity and Fracture," *J. Eng. Mat. Technol.*, **110**, 258 (July 1988).
Sydansk, R. D., "Foam for Improving Sweep Efficiency in Subterranean Oil-Bearing Formations," U.S. Patent 5 105 884 (Apr. 21, 1992).
Tonyan, T. D., and L. J. Gibson, "Structure and Mechanics of Cement Foams," *J. Mat. Sci.*, **27**, 6379 (1992a).
Tonyan, T. D., and L. J. Gibson, "Strengthening of Cement Foams," *J. Mat. Sci.*, **27**, 6371 (1992b).
Wilkinson, D., and J. F. Willemsen, "Invasion Percolation: A New Form of Percolation Theory," *J. Phys. A: Math. Gen.*, **16**, 3365 (1983).

Manuscript received Aug. 22, 1994, and revision received Dec. 5, 1994.